Delay-Dependent Stability of Load Frequency Control in Networked Power Systems Integrated with Electric Vehicles

K. Ramakrishnan * **A. Jawahar** *

* *Department of Electrical and Electronics Engineering, Puducherry Technological University, Puducherry, India (e-mail: ramakrishnan@ pec.edu, jawahar.a@pec.edu).*

Abstract: In this paper, impact of the integration of plug-in-electric vehicle units in enhancing the delay-dependent stability margin of a class of networked load frequency control systems is investigated using the classical Lyapunov-Krasovskii functional approach. In networked control systems, owing to the use of communication links, time-delays get introduced in the feedback path. These communication network-induced delays invariably exert a negative influence on system performance and stability. Furthermore, if the delay magnitude exceeds a critical margin, called stable delay margin, the system loses stability. In recent times, electric vehicle aggregators are integrated as a distributed generation source in the load frequency control systems for enhancing the grid frequency compensation. In such systems, in addition to improved frequency compensation, integration of electric vehicles also paves way in the enhancement of stable delay margin. To study this impact of integration of electric vehicle aggregators on stable delay margin, in this paper, two types of centralized load frequency control systems are considered. Furthermore, time-delays in the centralized control loop and electric vehicle aggregator loop are considered to be non-identical, and appropriate participation factors for effective load sharing are incorporated in the system framework.

Keywords: Load Frequency Control Systems, Micro-grid, Time-delay, Electric Vehicles, Delay-dependent Stability, Linear Matrix Inequality.

1. INTRODUCTION

In recent times, plug-in-electric vehicles (PEVs) are integrated into the load frequency control (LFC) scheme of power system as a distributed generation source for enhancing its frequency compensation capability; see, Kempton (1997); Liu et. al. (2013); Masuta and Yokoyama (2012); Green et. al. (2011); H Gunduz et.al. (2022); A.Naveed et.al. (2022); M. A. Hernández-Pérez et.al. (2018). In the event of main grid going down, the internal battery of the electric vehicle (EV) is called for to supply backup power as well as provide the much required voltage support to prevent momentary lapses in electricity; see, Peterson et. al. (2011); Yilmaz and Krien (2013). The vehicle-to-grid (VTG) technology enables bidirectional active and reactive power transfer between EVs and power system grid; see, Sortomme and El-Sharkwi (2011, 2012,a); Yilmaz and Krien (2015). In recent days, the EV concept is mostly implemented by EV aggregators (EVA) that encompass a fleet of electric vehicles parked all the day with their internal batteries capable enough to supplement power contribution; see, Tomic and Kempton (2007); Oretega et. al. (2013); Naveed et. al. (2021) and the references cited therein. Apart from frequency compensation, the major advantage that these electrical mobility systems offer is secure de-carbonization of the electricity grid; see, Boran et. al. (2017). In micro-grid framework, the PEVs operate in tandem with the other connected distributed generation units in compensating the grid frequency against unplanned outages; invariably, they offer resilience for critical and non-critical loads in a staged approach that lowers costs and spreads those costs over longer operating periods; see, Vachirasricirikul and Ngamroo (2014). High penetration of renewable energy requires consistent energy storage, which electric vehicles can provide with consummate ease. The EVs have the potential to provide the much needed storage feature. However, they present unique challenges in that they are neither stationed in fixed locations nor continuously connected to the grid; nevertheless, they are expected to cater transportation requirements as well. Refer, Grosjean et. al. (2012); Fox (2013); Ana Paula Batista et.al. (2014).

In such integrated power systems, since balancing between the total generation against total demand including the system losses is a major issue, the load frequency control problem has been extensively investigated in the recent years; refer, Vijay Singh et. al. (2016); Ko and Sung (2018); Han et. al. (2018) and the references cited therein. In case of a sudden load change, the power system operating point experiences a perturbation. This, in turn, causes a deviation in the system frequency and the scheduled tie-line power flow from their nominal values. As a follow-up action, the load frequency control scheme, from the feedback of the area control error (ACE) variable, achieves the power balance between the interconnected areas thereby restoring the system frequency closer to the

nominal value and tie-line power flow to its scheduled value; refer, Kundur (1994); Elgerd (1971); Q.Hai (2021). This necessitates the use of communication channels for connecting the sensors (phasor measurement units), actuators and controllers in order to control the power output from the generation units that are dispersed geographically; see, Tani et. al. (2015). This paves way to the emergence of time-delay in the feedback loop of the control system. The networked operation of load frequency control in the conventional power systems relies on the communication links which causes inevitable delays in the feedback loops leading to delay induced stability issues. In a centrally controlled micro-grid system that includes various distributed generation units, time-delay is ubiquitous in the signal communication process. In both the cases, the existence of network-induced delays imposes constraint on the transmission of information among different entities involved in the control task. Under worst case operating scenario, the measurement and control signals in the form of information packets may be completely lost in the transmission channels. The time-delay, that depends on the communication network bandwidth, distance and packet drop outs invariably affects the overall performance and stability of the overall system. Depending upon the use of dedicated or open type communication channels, the network-induced time-delays can be either constant or time-varying respectively. For LFC systems with a single constant delay, stability is assessed from the computation of critical eigen values. For systems with multiple time-invariant delays or with time-varying delays, Lyapunov-Krasovskii (LK) stability theory and linear matrix inequality (LMI) techniques are employed to compute the stable delay margin ; see, S.B.Pandu et.al. (2022); Ana Paula Batista et.al. (2014). In the Lyapunov indirect technique, a positive definite LK functional that depicts the energy of the perturbed system is constructed, and the time-derivative of the functional is bounded using appropriate bounding techniques in a less conservative manner. The resulting stability criterion is generally expressed as a set of LMI conditions that can be solved readily using standard numerical packages; refer, Gahi et. al. (1995). The conservatism in the stability analysis depends on the choice of the LK functional and the techniques used for bounding the time-derivative of the functional.

In this paper, two types of centralized load frequency control systems integrated with electric vehicle aggregators are investigated. The first scheme involves the conventional power system grid and the second one considers a micro-grid system. The schemes are detailed in the following subsections.

1.1 LFC System with EV Aggregator

The block diagram of ith unit of a generalized multi-area load frequency control system with tie-line power feeds is shown in Fig. 1. In the event of generation-demand imbalance in power system grid, the controller, based on the feedback of incremental frequency variable Δf_i and incremental tie-line power variable $\Delta P_{tie,i}$, initiates the control action to restore the balance. The feedback variable Area Control Error (ACE) is processed by the controller, and the control effort is routed through communication channels with appropriate participation factors $\alpha_{PS,i}$ and

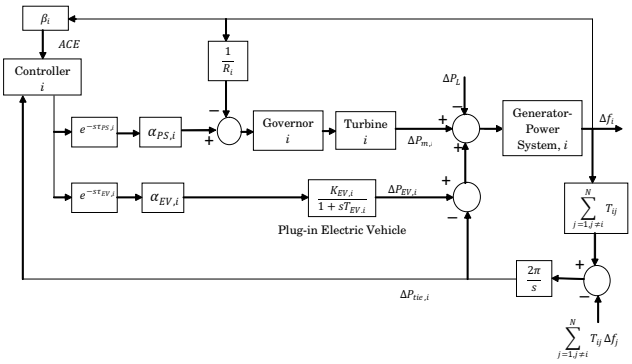

Fig. 1. Multi-area Load Frequency Control System.

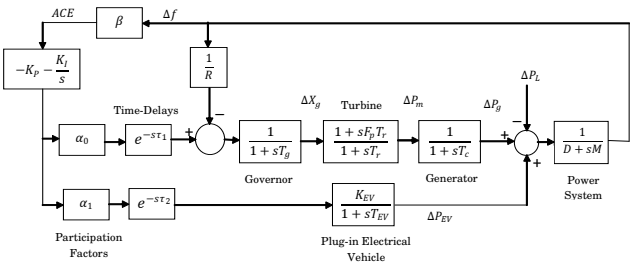

Fig. 2. Single Area Load Frequency Control System with EV Integration.

$\alpha_{EV,i}$ that decide the sharing of excess/deficit load by the conventional power generation and EV. The time-delays induced by the communication channels are depicted as $\tau_{PS,i}$ and $\tau_{EV,i}$ for the conventional generation units and EV units respectively. In real time operating conditions, these delays are dissimilar or incommensurate in nature. The transfer function of EV is usually first order and is given by

$$G_{EV}(s) = \frac{K_{EV}}{1 + sT_{EV}} \tag{1}$$

where K_{EV} is the gain of EV and T_{EV} is the time constant of EV. A typical case of a single area LFC system integrated with EV is shown in Fig. 2 where various subsystems in the load frequency control are modeled as first order transfer functions and the control logic is of PI type; refer Ko and Sung (2018) for a detailed description on system variables and parameters.

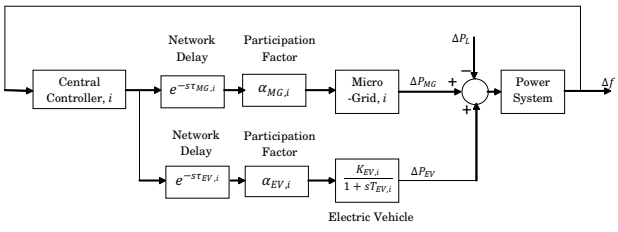

Fig. 3. Block Diagram of Networked Micro-Grid System.

1.2 Micro-grid System with EV Aggregator

The block diagram of a micro-grid system with EV aggregator is shown in Fig. 3 where ΔP_{MG} and ΔP_{EV} are the incremental power contributed by micro-grid and electric vehicle aggregator for an incremental load change ΔP_L

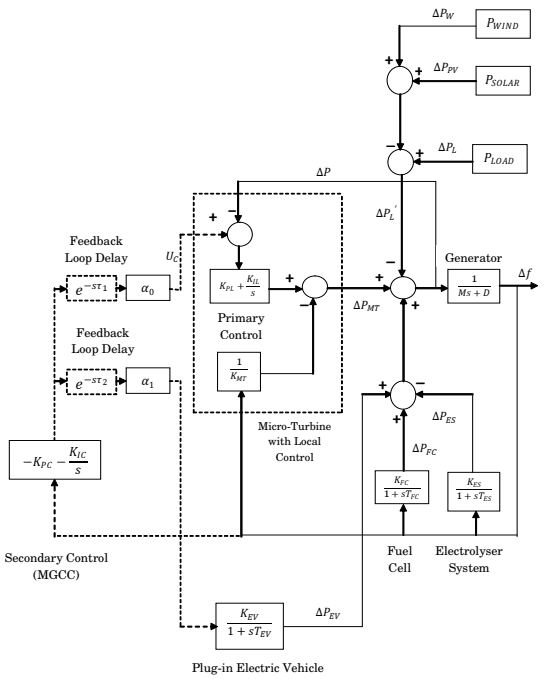

Fig. 4. Micro-grid Load Frequency Control System with EV Integration.

which is identified by a variation in system frequency Δf. Similar to the description presented in the previous section τ_{MG} and τ_{EV} represent respective time-delays in the micro-grid and EV loops. Similarly, the participation factors are represented as α_{MG} and α_{EV} in micro-grid and EV feedback loops respectively. A typical micro-grid system with two time-delays is shown in Fig. 4. The building blocks of this time-delayed micro-grid model are taken from Gunduz et. al. (2017). In this scheme, fuel cell with electrolyzer and micro-turbine with localized controller are the primary distributed generation units in the micro-grid. The supplement power contribution to the grid is obtained from the EVA integrated to the system. A centralized controller (PI control logic) through communication channels controls the overall system to ensure power balance in case of increase or decrease in load. The time-delays in the communication channels are τ_1 and τ_2 for the main distributed sources and EVA respectively. These delays are considered to be dissimilar. Appropriate participation factors α_0 and α_1 decide the ratio of load sharing.

In literature, there are only few results reported on the stability issues in EVA integrated LFC systems in a multiple time-delay environment. In Ko and Sung (2018), multiple time-delays are considered only in EVA aggregators, and time-delay normally encountered in conventional power generation path is not taken into consideration. Subsequently, using a previously reported result in Ko et. al. (2018), the stable delay margin is obtained for the multiple time-delayed LFC system. In Naveed et. al. (2020), a single time-invariant delay in EVA loop is considered, and using the transcendental characteristic equation approach Sonmez et. al. (2016), delay-dependent stability and stabilizing region in controller parametric space is obtained for different values of loop delays. In Naveed et. al. (2019), incommensurate time-delays are considered in conventional power generation path and EVA loop, and stabilizing region in centralized PI controller parametric space is obtained. In Gunduz et. al. (2019), the EVA integration with micro-grid is considered with a common single time-delay element, and stabilizing region in controller parametric space is obtained. To the best of our knowledge, delay-dependent stability problem of both the classical load frequency control systems and micro-grid systems involving dissimilar time-delays in conventional power generation path and EVA loop has not been addressed comprehensively using Lyapunov techniques in literature so far.

In this paper, using a novel Lyapunov-Krasovskii functional based analysis that employs Wirtinter inequality, delay-dependent stability is ascertained for EV integrated LFC and micro-grid systems with dissimilar time-delays in conventional power generation and EVA loops.

1.3 State Space Model of Conventional LFC System with EVA

For analyzing stability, the mathematical model of the conventional single area LFC system integrated with EVA shown in Fig. 2 is expressed as follows:

$$\dot{x}(t) = Ax(t) + A_{d1}x(t-\tau_1) + A_{d2}x(t-\tau_2), \tag{2}$$

$$x(t) = \Phi(t), \forall t \in [-\max(\tau_1, \tau_2),\ 0], \tag{3}$$

where $x(t) \in \mathbb{R}^{6\times 1}$ is the state vector, and A, A_{d1} and A_{d2} are the system matrices associated with current state vector and delayed state vectors. τ_1 and τ_2 are the time-delays associated with the system. These delays are assumed to have dissimilar characteristics. Hence, $\tau_1 \neq \tau_2$. The state vector is given by $x(t) = [\Delta f(t)\ \ \Delta P_g(t)\ \ \Delta P_m(t)\ \ \Delta X_g(t)\ \ ACE(t)\ \ \Delta P_{EV}(t)]^T$ and system matrices are as follows:

$$A = \begin{bmatrix} -\frac{D}{M} & \frac{1}{M} & 0 & 0 & 0 & \frac{1}{M} \\ 0 & -\frac{1}{T_c} & \frac{1}{T_c} & 0 & 0 & 0 \\ -\frac{F_p}{RT_g} & 0 & -\frac{1}{T_r} & -\frac{F_p}{T_g}+\frac{1}{T_r} & 0 & 0 \\ -\frac{1}{RT_g} & 0 & 0 & -\frac{1}{T_g} & 0 & 0 \\ \beta & 0 & 0 & 0 & 0 & 0 \\ 0 & 0 & 0 & 0 & 0 & -\frac{1}{T_{EV}} \end{bmatrix}, \tag{4}$$

$$A_{d1} = \begin{bmatrix} 0 & 0\ 0\ 0 & 0 & 0 \\ 0 & 0\ 0\ 0 & 0 & 0 \\ -\frac{\alpha_0 F_p \beta K_P}{T_g} & 0\ 0\ 0 & -\frac{\alpha_0 F_p K_I}{T_g} & 0 \\ -\frac{\alpha_0 \beta K_P}{T_g} & 0\ 0\ 0 & -\frac{\alpha_0 K_I}{T_g} & 0 \\ 0 & 0\ 0\ 0 & 0 & 0 \\ 0 & 0\ 0\ 0 & 0 & 0 \end{bmatrix}, \tag{5}$$

$$A_{d2} = \begin{bmatrix} 0 & 0\ 0\ 0 & 0 & 0 \\ 0 & 0\ 0\ 0 & 0 & 0 \\ 0 & 0\ 0\ 0 & 0 & 0 \\ 0 & 0\ 0\ 0 & 0 & 0 \\ 0 & 0\ 0\ 0 & 0 & 0 \\ -\frac{\alpha_1 K_{EV} \beta K_P}{T_{EV}} & 0\ 0\ 0 & -\frac{\alpha_1 K_{EV} K_I}{T_{EV}} & 0 \end{bmatrix}. \tag{6}$$

1.4 State Space Model of Micro-grid LFC System with EVA

The micro-grid system can also be modelled in state space approach as given in (2) and (3). For the networked micro-grid system shown in Fig. 3, the state vector is given by $x(t) = [\Delta f(t) \quad \Delta P_{MT}(t) \quad \Delta P_{FC}(t) \quad \Delta P_{ES}(t) \quad \int \Delta f(t)dt \quad \Delta P_{EV}(t)]^T$. The corresponding system matrices are given below:

$$A = \begin{bmatrix} -\frac{D}{M} & \frac{1}{M} & \frac{1}{M} & -\frac{1}{M} & 0 & \frac{1}{M} \\ a_{21} & a_{22} & a_{23} & a_{24} & a_{25} & a_{26} \\ \frac{K_{FC}}{T_{FC}} & 0 & -\frac{1}{T_{FC}} & 0 & 0 & 0 \\ \frac{K_{ES}}{T_{ES}} & 0 & 0 & -\frac{1}{T_{ES}} & 0 & 0 \\ 1 & 0 & 0 & 0 & 0 & 0 \\ 0 & 0 & 0 & 0 & 0 & -\frac{1}{T_{EV}} \end{bmatrix}, \quad (7)$$

$$A_{d1} = \begin{bmatrix} 0 & 0 & 0 & 0 & 0 & 0 \\ b_{21} & b_{22} & b_{23} & b_{24} & b_{25} & b_{26} \\ 0 & 0 & 0 & 0 & 0 & 0 \\ 0 & 0 & 0 & 0 & 0 & 0 \\ 0 & 0 & 0 & 0 & 0 & 0 \\ 0 & 0 & 0 & 0 & 0 & 0 \end{bmatrix}, \quad (8)$$

$$A_{d2} = \begin{bmatrix} 0 & 0 & 0 & 0 & 0 & 0 \\ c_{21} & 0 & 0 & 0 & c_{25} & 0 \\ 0 & 0 & 0 & 0 & 0 & 0 \\ 0 & 0 & 0 & 0 & 0 & 0 \\ 0 & 0 & 0 & 0 & 0 & 0 \\ c_{61} & 0 & 0 & 0 & c_{65} & 0 \end{bmatrix}, \quad (9)$$

where

$$a_{21} = \frac{1}{(1+K_{PL})}\left[\frac{D}{MK_{MT}} - \frac{K_{PL}K_{FC}}{T_{FC}} + \frac{K_{PL}K_{ES}}{T_{ES}}\right],$$
$$a_{22} = \frac{1}{(1+K_{PL})}\left[\frac{-1}{MK_{MT}} - K_{IL}\right],$$
$$a_{23} = \frac{1}{(1+K_{PL})}\left[\frac{-1}{MK_{MT}} + \frac{K_{PL}}{T_{FC}} - K_{IL}\right],$$
$$a_{24} = \frac{1}{(1+K_{PL})}\left[\frac{1}{MK_{MT}} - \frac{K_{PL}}{T_{ES}} + K_{IL}\right],$$
$$a_{25} = 0,$$
$$a_{26} = \frac{1}{(1+K_{PL})}\left[\frac{-1}{MK_{MT}} - K_{IL} + \frac{K_{PL}}{T_{EV}}\right],$$
$$b_{21} = \frac{1}{(1+K_{PL})}\left[\frac{\alpha_0 DK_{PC}K_{PL}}{M} - \alpha_0 K_{PL}K_{IC} - \alpha_0 K_{IL}K_{PC}\right],$$
$$b_{22} = \frac{1}{(1+K_{PL})}\left[\frac{-\alpha_0 K_{PC}K_{PL}}{M}\right],$$
$$b_{23} = \frac{1}{(1+K_{PL})}\left[\frac{-\alpha_0 K_{PC}K_{PL}}{M}\right],$$
$$b_{24} = \frac{1}{(1+K_{PL})}\left[\frac{\alpha_0 K_{PC}K_{PL}}{M}\right],$$
$$b_{25} = \frac{1}{(1+K_{PL})}\left[-\alpha_0 K_{IC}K_{IL}\right],$$
$$b_{26} = \frac{1}{(1+K_{PL})}\left[\frac{-\alpha_0 K_{PC}K_{PL}}{M}\right],$$
$$c_{21} = \frac{1}{(1+K_{PL})}\left[\frac{\alpha_1 K_{PC}K_{PL}K_{EV}}{T_{EV}}\right],$$
$$c_{25} = \frac{1}{(1+K_{PL})}\left[\frac{\alpha_1 K_{IC}K_{PL}K_{EV}}{T_{EV}}\right],$$
$$c_{61} = \frac{-\alpha_1 K_{PC}K_{EV}}{T_{EV}},$$
$$c_{65} = \frac{-\alpha_1 K_{IC}K_{EV}}{T_{EV}}.$$

The delays $\tau_i \in \mathbb{R}^+$, $i = 1,\ 2$ are constant time-delays in the feedback loops of the micro-grid system. The delays are dissimilar. The initial condition of the system given by $\Phi(t)$ is a continuous-time function. The problem addressed in this paper is stated below:

Delay-Dependent Stability Problem: *To develop a less conservative stability criterion in LMI framework to compute the maximum allowable bound of the time-delays τ_i, $i = 1,\ 2$ within which the conventional LFC and micro-grid systems integrated with EVA described by (2) remains asymptotically stable in the sense of Lyapunov for the given initial condition (3) using Lyapunov-Krasovskii functional approach combined with Jenson integral inequality Zhu and Yang (2008) and Wirtinger inequality Sauret and Gouaisbaut (2011).* Refer, Ramakrishnan and Jawahar (2011).

Lemma 1. ***Jenson Integral Inequality*** *(Zhu and Yang (2008)) For any positive symmetric constant matrix $M \in \mathbb{R}^{n\times n}$, scalars r_1 and r_2 satisfying $r_1 < r_2$, a vector valued function $\omega :\ [r_1,\ r_2] \to \mathbb{R}^n$ such that the integrations concerned are well defined, then the inequality (10) holds.*

Lemma 2. ***Wirtinger Inequality*** *(Sauret and Gouaisbaut (2011)): For given symmetric positive definite matrix R, and for any differentiable signal ω in $[a,\ b] \to \mathcal{R}^n$, then the inequality (11) holds.*

2. MAIN RESULT

Based on the discussion presented in the last two subsections, for N-area systems, the mathematical model of the conventional and micro-grid based LFC system can be derived in the following generalized framework:

$$\dot{x}(t) = Ax(t) + \sum_{i=1}^{N} A_i x(t-\tau_i), \quad (12)$$

$$x(t) = \phi(t),\ \forall\ t \in [-\max(\tau_i), 0],\ i = 1,\ 2,\ \ldots,\ N \quad (13)$$

where $x(t) \in \mathbb{R}^{n\times 1}$ is the state vector and $A \in \mathbb{R}^{n\times n}$ and $A_i \in \mathbb{R}^{n\times n}$, $i = 1,\ 2,\ \ldots,\ N$ are the system matrices associated with current and delayed state vectors; The N time-invariant delays satisfy $0 \le \tau_i \le \bar{\tau}_i$. The proposed delay-dependent stability criterion for the multiple time-delayed system (12) is presented in the following theorem.

Theorem 3. The system (12) with N non-identical time-delays satisfying (13) is asymptotically stable in the sense of Lyapunov if there exists real symmetric positive definite matrices P_{11}, S_k, R_k, $k = 1$ to N, and R_{ij}, $i = 1$ to $(N-1)$ and $j = i+1$ to N; symmetric matrices P_{mm}, $m = 2$ to $(N+1)$; free matrices P_{ij}, $i = 1$ to N and $j = i+1$ to $N+1$ such that following LMIs hold:

$$\Pi_0 \ge 0, \quad (14)$$

$$\begin{bmatrix} \sum_{k=1}^{5} \Pi_k & \bar{A}^T U_1 & \bar{A}^T U_2 \\ \star & -U_1 & 0 \\ \star & \star & -U_2 \end{bmatrix} < 0, \quad (15)$$

$$\left(\int_{r_1}^{r_2}\omega(s)ds\right)^T M\left(\int_{r_1}^{r_2}\omega(s)ds\right) \le (r_2-r_1)\int_{r_1}^{r_2}\omega^T(s)M\omega(s)ds. \tag{10}$$

$$\int_b^a \dot{\omega}^T(u)R\dot{\omega}(u)du \ge \frac{1}{b-a}\begin{bmatrix}\omega(b)\\ \omega(a)\\ \frac{1}{b-a}\int_a^b\omega(u)du\end{bmatrix}^T\begin{bmatrix}4R & 2R & -6R\\ \star & 4R & -6R\\ \star & \star & 12R\end{bmatrix}\begin{bmatrix}\omega(b)\\ \omega(a)\\ \frac{1}{b-a}\int_a^b\omega(u)du\end{bmatrix}. \tag{11}$$

$$\Pi_3 = \left[\begin{array}{ccccccc|cccc}
\sum_{i=1}^{N}\frac{-4}{\tau_i}R_i & -\frac{2}{\tau_1}R_1 & -\frac{2}{\tau_2}R_2 & -\frac{2}{\tau_3}R_3 & \dots & -\frac{2}{\tau_N}R_N & \frac{6}{\tau_1}R_1 & \frac{6}{\tau_2}R_2 & \frac{6}{\tau_3}R_3 & \dots & \frac{6}{\tau_N}R_N\\
\star & -\frac{4}{\tau_1}R_1 & 0 & 0 & \dots & 0 & \frac{6}{\tau_1}R_1 & 0 & 0 & \dots & 0\\
\star & \star & -\frac{4}{\tau_2}R_2 & 0 & \dots & 0 & 0 & \frac{6}{\tau_2}R_2 & 0 & \dots & 0\\
\star & \star & \star & -\frac{4}{\tau_3}R_3 & \dots & 0 & 0 & 0 & \frac{6}{\tau_3}R_3 & \dots & 0\\
\vdots & \vdots & \vdots & \vdots & \dots & \vdots & \vdots & \vdots & \vdots & \dots & \vdots\\
\star & \star & \star & \star & \dots & -\frac{4}{\tau_N}R_N & 0 & 0 & 0 & \dots & \frac{6}{\tau_N}R_N\\
\hline
\star & \star & \star & \star & \dots & \star & -\frac{12}{\tau_1}R_1 & 0 & 0 & \dots & 0\\
\star & \star & \star & \star & \dots & \star & \star & -\frac{12}{\tau_2}R_2 & 0 & \dots & 0\\
\star & \star & \star & \star & \dots & \star & \star & \star & -\frac{12}{\tau_3}R_3 & \dots & 0\\
\vdots & \vdots & \vdots & \vdots & \dots & \vdots & \vdots & \vdots & \vdots & \dots & \vdots\\
\star & \star & \star & \star & \dots & \star & \star & \star & \star & \dots & -\frac{12}{\tau_N}R_N
\end{array}\right].$$

where the elements of the linear matrix inequalities (14) and (15) are given below. In these matrices, the $\star$ represents the symmetric elements in the symmetric matrix and $diag([\cdot])$ represents diagonal matrix.

$$\Pi_0 = P + diag([0, \tau_1^{-1}S_1,\ \tau_2^{-1}S_2,\ \tau_3^{-1}S_3,\ \dots,\ \tau_N^{-1}S_N])$$

$$\Pi_1 = \Phi_1^T P\Phi_2 + (\Phi_1^T P\Phi_2)^T,$$

$$\Pi_2 = diag([\sum_{i=1}^{N}S_i,\ -S_1,\ -S_2,\ -S_3,\ \dots,\ -S_N,\ \underbrace{0,\ 0,\ 0,\ \dots,0}_{N}]),$$

$$\Pi_4 = \begin{bmatrix}\Pi_5 & 0_{N\times N}\\ \star & 0_{N\times N}\end{bmatrix},$$

$$\Pi_5 = \begin{bmatrix}0 & 0 & 0 & 0 & \dots & 0\\ \star & \Gamma_{22} & R_{12} & R_{13} & \dots & R_{1N}\\ \star & \star & \Gamma_{33} & R_{23} & \dots & R_{2N}\\ \star & \star & \star & \Gamma_{44} & \dots & R_{3N}\\ \vdots & \vdots & \vdots & \vdots & \dots & \vdots\\ \star & \star & \star & \star & \dots & \Gamma_{N+1,N+1}\end{bmatrix},$$

with

$$\Gamma_{i+1,i+1} = \sum_{j=1}^{i-1}R_{ji} + \sum_{j=i+1}^{N}R_{ij},$$

and

$$P = \begin{bmatrix}P_{11} & P_{12} & P_{13} & \dots & P_{1,N+1}\\ \star & P_{22} & P_{23} & \dots & P_{2,N+1}\\ \star & \star & P_{33} & \dots & P_{3,N+1}\\ \vdots & \vdots & \vdots & \dots & \vdots\\ \star & \star & \star & \dots & P_{N+1,N+1}\end{bmatrix},$$

$$\Phi_1 = \left[\begin{array}{c|c}I_{n\times n} & 0_{n\times nN}\\ \hline 0_{nN\times n} & 0_{nN\times nN}\\ \hline 0_{nN\times n} & diag([\tau_1,\ \tau_2,\ \tau_3,\ \dots,\tau_N])\end{array}\right],$$

$$\Phi_2 = \begin{bmatrix}A & A_1 & A_2 & A_3 & \dots & A_N & 0 & 0 & 0 & \dots & 0\\ I & -I & 0 & 0 & \dots & 0 & 0 & 0 & 0 & \dots & 0\\ I & 0 & -I & 0 & \dots & 0 & 0 & 0 & 0 & \dots & 0\\ I & 0 & 0 & -I & \dots & 0 & 0 & 0 & 0 & \dots & 0\\ \vdots & \vdots & \vdots & \vdots & \dots & \vdots & \vdots & \vdots & \vdots & \dots & \vdots\\ I & 0 & 0 & 0 & \dots & -I & 0 & 0 & 0 & \dots & 0\end{bmatrix},$$

$$\bar{A} = [\,A\ A_1\ A_2\ \dots\ A_N\ 0\ 0\ \dots\ 0\,]$$

$$U_1 = \sum_{i=1}^{N}\tau_i R_i,$$

$$U_2 = \sum_{i=1}^{N-1}\sum_{j=i+1}^{N}(\tau_j-\tau_i)^2 R_{ij}.$$

The proof is based on Lyapunov-Krasovskii approach.

Proof. The proposed stability criterion is derived using the Lyapunov-Krasovskii functional $V(x(t)) = \sum_{i=1}^{4} V_i(x(t))$ with

$$V_1(x(t)) = \Xi^T(t) P \Xi(t), \tag{16}$$

$$V_2(x(t)) = \sum_{i=1}^{N} \int_{t-\tau_i}^{t} x^T(s) S_i x(s) ds, \tag{17}$$

$$V_3(x(t)) = \sum_{i=1}^{N} \int_{-\tau_i}^{0} \int_{t+\theta}^{t} \dot{x}^T(s) R_i \dot{x}(s) ds d\theta, \tag{18}$$

$$V_4(x(t)) = \sum_{i=1}^{N-1} \sum_{j=i+1}^{N} (\tau_j - \tau_i) \int_{-\tau_j}^{-\tau_i} \int_{t+\theta}^{t} \dot{x}^T(s) R_{ij} \dot{x}(s) ds d\theta, \tag{19}$$

where $\Xi(t) = [x^T(t) \quad \int_{t-\tau_1}^{t} x^T(s) ds \quad \int_{t-\tau_2}^{t} x^T(s) ds \quad . \quad . \quad \int_{t-\tau_N}^{t} x^T(s) ds]^T$. By Jenson's integral inequality, following conditions hold good for $i = 1$ to N:

$$\int_{t-\tau_i}^{t} x^T(s) S_i x(s) ds \geq \Big[\int_{t-\tau_i}^{t} x(s) ds \Big]^T \Big(\frac{S_i}{\tau_i} \Big) \Big[\int_{t-\tau_i}^{t} x(s) ds \Big], \tag{20}$$

By using the above set of equations (20), one can readily obtain a lower bound for $V(x(t))$ as follows:

$$V(x(t)) \geq \Xi(t)^T \Pi_0 \Xi(t) + V_3(x(t)) + V_4(x(t)). \tag{21}$$

Now, it is clear that positive definiteness of the matrices P, S_i, $i = 1, 2, \ldots N$; R_{ij}; $i = 1, 2, \ldots N-1$ and $j = i+1, i+2, \ldots N$ and $\Pi_0 > 0$ (equation (14)) implies positive definiteness of $V(x(t))$. This paves way to a less conservative solution as detailed in Sauret and Gouaisbaut (2011). The time-derivative of the functional $V_1(x(t))$ along the trajectory of (2) is given by

$$\dot{V}_1(x(t)) = 2\Xi^T(t) P \dot{\Xi}(t), \tag{22}$$

which can be rewritten as follows:

$$\dot{V}_1(x(t)) = \delta^T(t) \Pi_1 \delta(t), \tag{23}$$

where $\delta(t) = [x^T(t) \quad x^T(t-\tau_1) \quad x^T(t-\tau_2) \quad \ldots x^T(t-\tau_N) \quad \frac{1}{\tau_1}\int_{t-\tau_1}^{t} x^T(s) ds \quad \frac{1}{\tau_2}\int_{t-\tau_2}^{t} x^T(s) ds \quad . \quad . \quad . \quad \frac{1}{\tau_N}\int_{t-\tau_N}^{t} x^T(s) ds]^T$ is an augmented state vector. The time-derivative of the functional $V_2(x(t))$ along (2) is given by

$$\dot{V}_2(x(t)) = x^T(t) \Big(\sum_{i=1}^{N} S_i \Big) x(t) - \sum_{i=1}^{N} x^T(t-\tau_i) S_i x(t-\tau_i); \tag{24}$$

the equation (24), in terms of $\delta(t)$, is expressed as follows:

$$\dot{V}_2(x(t)) = \delta^T(t) \Pi_2 \delta(t). \tag{25}$$

The time-derivative of the functional $V_3(x(t)$ along (2) is given by

$$\dot{V}_3(x(t)) = \dot{x}^T(t) U_1 \dot{x}(t) - \sum_{i=1}^{N} \Big(\int_{t-\tau_i}^{t} \dot{x}^T(s) R_i \dot{x}(s) ds \Big). \tag{26}$$

Now, by using Wirtinger inequality, the equation (26) is expressed as an inequality as follows:

$$\dot{V}_3(x(t)) \leq \delta^T(t) (\bar{A}^T U_1 \bar{A}) \delta(t) + \delta^T(t) \Pi_3 \delta(t) + \delta^T(t) \Pi_4 \delta(t). \tag{27}$$

The time-derivative of $V_4(x(t)$ along (2) is given by

$$\dot{V}_4(x(t)) = \dot{x}^T(t) U_2 \dot{x}(t) - \sum_{i=1}^{N-1} \sum_{j=i+1}^{N} (\tau_j - \tau_i) \int_{t-\tau_j}^{t-\tau_i} \dot{x}^T(s) R_{ij} \dot{x}(s) ds. \tag{28}$$

Now, by using Jenson's integral inequality, the equation (28) is expressed as an inequality as follows:

$$\dot{V}_4(x(t)) \leq \delta^T(t) (\bar{A}^T U_2 \bar{A}) \delta(t) + \delta^T(t) \Pi_5 \delta(t). \tag{29}$$

By combining the time-derivative of the LK functionals $\dot{V}_i(x(t))$, $i = 1$ to 4, we get the following condition:

$$\dot{V}(x(t)) = \sum_{i=1}^{4} \dot{V}_i(x(t)) \leq \delta^T(t) \Big[\sum_{k=1}^{5} \Pi_k + \bar{A}^T (U_1 + U_2) \bar{A} \Big] \delta(t). \tag{30}$$

Now, by Schur complement, if the inequality conditions (14) and (15) hold simultaneously, then there exists a sufficiently small scalar $\alpha > 0$ such that $\dot{V}(x(t)) \leq -\alpha ||x(t)||^2$, which, in turn, implies that the LFC systems described by (12) with (13) are asymptotically stable in the sense of Lyapunov; refer, Gu and Niculescu (2003). This completes proof of the Theorem.

3. NUMERICAL EXAMPLE

3.1 System Parameters

For computing the stable delay margin, bench mark LFC and micro-grid systems are considered. The parameters of the systems are taken from Naveed et. al. (2019) for LFC system and Gunduz et. al. (2019) for micro-grid system. The parameters are listed in Table 1 and Table 2.

Table 1. Parameters of the LFC System

Parameter	Description	Value
M	Moment of inertia	8.8
D	Damping Coefficient	1
T_c	Time-Constant of Generator	0.3
T_g	Time-Constant of Governor	0.2
R	Derating Factor	$\frac{1}{11}$
β	ACE Feedback Factor	21
F_p	Reheat Turbine Gain	$\frac{1}{6}$
T_r	Reheat Turbine Time-Constant	12
K_{EV}	Gain of Electrical Vehicle	1
T_{EV}	Time-constant of Electrical Vehicle	0.1

3.2 Analytical Results for LFC System

The stable margin for time-delays obtained by the proposed stability criterion Theorem 1 are listed in Table 3 and Table 4 for LFC system for different subsets of the centralized PI controller parameters (K_P, K_I) (Boyd et. al. (1994)). The Table 3 gives stable delay margin for $\alpha_0 = 0.6$ and $\alpha_1 = 0.4$ and the Table 4 presents stable delay margin for $\alpha_0 = 0.8$ and $\alpha_1 = 0.2$. For computing the stable delay margin, the proportional gain is set at $K_P = 0.1$, and the integral gain K_I is varied as 0.1, 0.2,

Table 2. Parameters of Benchmark Micro-grid System

Parameter	Description	Value
M	Moment of inertia	10
D	Damping Coefficient	1
K_{MT}	Micro-turbine droop	0.04
K_{FC}	Gain of Fuel Cell	1
T_{FC}	Time-constant of Fuel Cell	4
K_{ES}	Gain of Electrolyzer system	1
T_{ES}	Time-constant of Electrolyzer system	1
K_{PL}	Proportional gain of Local Controller	1
K_{IL}	Integral gain of Local Controller	1
K_{EV}	Gain of Electrical Vehicle	22.1
T_{EV}	Time-constant of Electrical Vehicle	1

0.4, 0.5 0.6 and 0.8. In these tables, the multiple delays are expressed as $\tau_d = \sqrt{\tau_1^2 + \tau_2^2}$ and $\theta = \tan^{-1}(\frac{\tau_2}{\tau_1})$.

Table 3. Maximum bound τ_d for $\alpha_0 = 0.6$ and $\alpha_1 = 0.4$

$K_P = 0.1$	K_I					
θ	0.1	0.2	0.4	0.5	0.6	0.8
5	37.184	14.731	5.123	3.377	2.262	0.943
10	19.222	7.408	2.572	1.695	1.136	0.579
20	9.775	3.762	1.316	0.910	0.660	0.367
30	6.687	2.573	0.958	0.678	0.498	0.280
40	5.202	2.028	0.790	0.562	0.414	0.234
45	4.753	1.874	0.736	0.525	0.387	0.218
50	4.369	1.763	0.696	0.496	0.366	0.207
60	3.980	1.625	0.643	0.458	0.338	0.190
70	3.899	1.567	0.616	0.439	0.323	0.182
80	4.087	1.570	0.612	0.435	0.320	0.180
85	4.319	1.594	0.617	0.438	0.322	0.181

Table 4. Maximum bound τ_d for $\alpha_0 = 0.8$ and $\alpha_1 = 0.2$

$K_P = 0.1$	K_I					
θ	0.1	0.2	0.4	0.5	0.6	0.8
5	16.665	8.732	1.410	0.846	0.538	0.201
10	15.813	6.476	1.178	0.732	0.472	0.179
20	12.458	3.546	0.932	0.596	0.390	0.149
30	9.569	**2.606**	0.805	0.521	0.342	0.132
40	7.617	2.250	0.734	0.477	0.315	0.121
45	7.027	2.153	0.713	0.464	0.306	0.118
50	6.436	2.091	0.698	0.455	0.300	0.116
60	6.123	2.051	0.689	0.449	0.296	0.114
70	6.901	2.113	0.704	0.458	0.302	0.116
80	12.926	2.304	0.746	0.484	0.319	0.122
85	25.754	2.476	0.781	0.505	0.332	0.127

3.3 Simulation Results for LFC System

For time-domain simulation studies, a load perturbation of $\Delta P_L = 0.1pu$ magnitude step function is initiated at $t = 0$, and the evolution of the incremental frequency variable $\Delta f(t)$ with respect to time is observed for the time-delayed micro-grid system for $t > 0$ (Gahi et. al. (1995)). The controller parameters are set at $K_P = 0.1$ and $K_I = 0.2$. For these controller gains, and $\alpha_0 = 0.8$ and $\alpha_1 = 0.2$, the stable delay margin obtained from Table 4 is $\tau_d = 2.606$ for $\theta = 30^0$. If the feedback loops delays are set corresponding to this value, the LFC system is at the verge of instability and the incremental frequency variable $\Delta f(t)$ exhibits sustained oscillation with respect to time. If loop delays are set at a value less than the stable delay margin, say $\tau_d = 2.5$ at $\theta = 30^0$, the closed-loop system yields asymptotically stable response. For loop delays greater than the stable delay margin say $\tau_d = 2.7$ at $\theta = 30^0$, the closed-loop system loses stability and $\Delta f(t)$ evolves unboundedly with time. The simulation results are presented in Fig. 5 for stable, marginally stable and unstable operation respectively. The simulation results are found to be in close agreement with the analytical results.

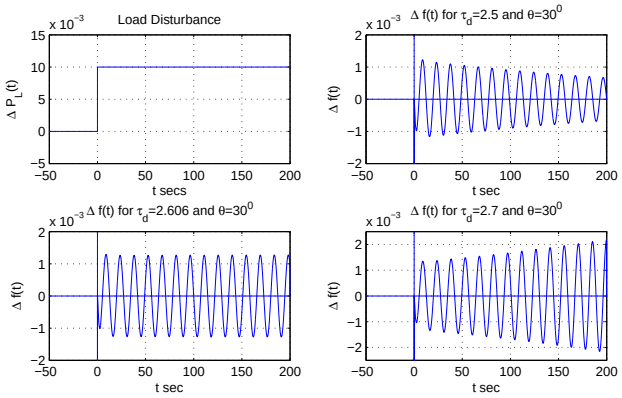

Fig. 5. Evolution of $\Delta f(t)$ for LFC System.

3.4 Analytical Results for Micro-Grid System

Similar to conventional load frequency control system, the stable margin for time-delays obtained by the proposed stability criterion Theorem 1 are listed in Table 5 and Table 6 for micro-grid system for different subsets of the MGCC PI controller parameters (K_{PC}, K_{IC}). The Table 5 gives stable delay margin for $\alpha_0 = 0.75$ and $\alpha_1 = 0.25$ and the Table 6 presents stable delay margin for $\alpha_0 = 0.9$ and $\alpha_1 = 0.1$.

3.5 Simulation Results for Micro-Grid System

For validating the analytical results, time-domain simulation studies are carried out for the micro-grid system to observe the evolution of the incremental frequency variable $\Delta f(t)$ for different time-delay values when the system is subjected to 0.1pu step load change. The controller parameters are set at $K_{PC} = 1$ and $K_{IC} = 0.6$. With these controller gains and $\alpha_0 = 0.75$ and $\alpha_1 = 0.25$, when $\theta = 30^0$, the closed-loop micro-grid system is stable up to a maximum delay bound of $\tau_d = 5.274$ (see, Table 5). For the delay value less than maximum delay bound, say, $\tau_d = 5$, the closed-loop system is stable with $\Delta f(t)$ variable converging asymptotically towards the equilibrium point

Table 5. Maximum bound τ_d for $\alpha_0 = 0.75$ and $\alpha_1 = 0.25$

$K_{PC} = 1$	K_{IC}				
θ	0.2	0.4	0.6	0.8	1.0
5	12.158	6.503	4.591	3.631	3.054
10	12.302	6.579	4.645	3.674	3.089
20	12.894	6.894	4.867	3.848	3.235
30	13.981	7.474	**5.274**	4.169	3.504
40	15.776	8.431	5.947	4.699	3.949
45	17.069	9.119	6.431	5.080	4.267
50	18.700	9.987	7.041	5.560	4.669
60	23.802	12.687	8.932	7.044	5.908
70	34.083	18.049	12.652	9.944	8.315
80	65.577	33.360	22.847	17.697	14.636
85	130.655	66.372	44.653	33.752	27.205

Table 6. Maximum bound τ_d for $\alpha_0 = 0.9$ and $\alpha_1 = 0.1$

$K_{PC} = 1$	K_{IC}				
θ	0.2	0.4	0.6	0.8	1.0
5	13.566	7.620	5.391	4.226	3.511
10	13.727	7.710	5.454	4.276	3.552
20	12.894	6.894	4.867	3.848	3.235
30	14.389	8.802	5.717	4.482	4.038
40	17.632	9.905	7.006	5.491	4.561
45	19.093	10.725	7.586	5.945	4.937
50	20.965	11.773	8.326	6.525	5.418
60	26.822	15.058	10.644	8.337	6.921
70	38.886	21.775	15.364	12.016	9.962
80	76.422	42.401	29.633	22.961	18.884
85	152.262	84.481	59.041	45.748	37.587

$\Delta f_e = 0$. It the delay margin is exactly set at $\tau_d = 5.274$, the system exhibits marginally stable response (sustained oscillations about the equilibrium point). If the delay value is increased to $\tau_d = 5.5$ which is more than the stable delay margin, the incremental frequency variable $\Delta f(t)$ evolves unboundedly with time signifying an unstable operating condition. All the simulation results are shown in Fig. 6 along with the step load disturbance. Hence, for micro-grid system also, the simulation results are in good agreement with the analytical results.

4. CONCLUSION

In this paper, two major types of networked load frequency control systems are considered with one involving the conventional power generation units and another one encompassing distributed generation in a micro-grid framework for investigating the impact of electric vehicle integration on stable delay margin. Plug-in electric vehicle with its efficient storage capability have become a new entity in micro-grids as well as in conventional large scale power system networks. The geographically dispersed nature of the electric vehicles makes them a viable option for supplementing the power grid in the event of increase in the demand of power by the connected loads. In days to come,

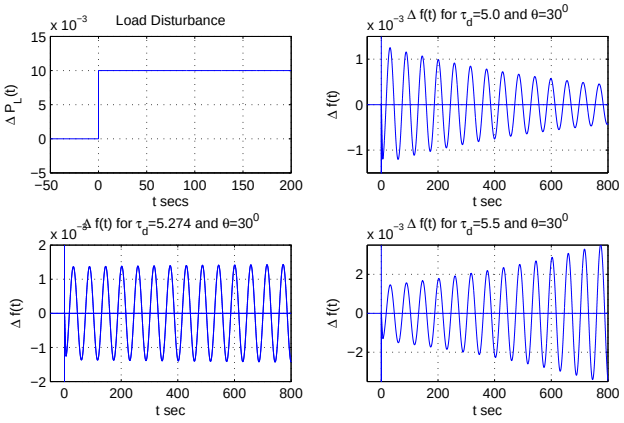

Fig. 6. Evolution of $\Delta f(t)$ for Micro-grid Systems.

the integration of the electric vehicle in modern power grids will increase drastically replacing in the process some of the conventional distributed generation units. The load frequency control systems are modelled as a linear retarded delay-differential equation involving two dissimilar time-delays in state space formulation. Using a new Lyapunov-Krasovskii functional combined with Wirtinger inequality, a less conservative delay-dependent stability criterion is derived in LMI framework. By solving the criterion, stable delay margins are computed for the LFC systems for different subsets of the controller parameters and participation factors. The proposed stability criterion is tested on standard benchmark systems, and subsequently, simulation results are presented to corroborate the analytical results. The possibility of extending the presented approach for the uncertain system with parametric uncertainties or exogenous noise will be explored in future.

REFERENCES

Boran Morvij, Ralph Evins and Jan Carmeliet. Decarbonizing the electricity grid: The impact on urban energy systems, distribution grids and direct heating potential. *Applied Energy*, 191:125–140, 2017.

G. H. Fox. Electric vehicle charging stations: Are we prepared? *IEEE Industry Applications Magazine*, 19(4): 32–38, 2013.

P. Gahinet, A. Nemirovskii, A. J. Laub and M. Chilali. *LMI Control Toolbox for use with MATLAB*. Mathworks, 1995.

R. C. Green, L. Wang, and N. Alam. Impact of plug-in hybrid electric vehicles on distributed networks: A review and outlook. *Renewable and Sustainable Energy Review*, 15(1):544–553, 2011.

C. Grosjean, P. H. Miranda, M. Perrin M and P Poggi. Assessment of world lithium resources and consequences of their geographic distribution on expected development of electric vehicle industry. *Renewable and Sustainable Energy Review*, 16(3):1735–1744, 2012.

K. Gu and I. Niculescu. Survey on Recent Results in the Stability and Control of Time-Delay Systems. *Journal of Dynamic Systems, Measurement, and Control*, 125: 1–8, 2003.

H. Gunduz, S. Sonmez and S. Ayasun. Comprehensive gain and phase margins based stability analysis of micro-grid frequency control system with constant communication

time delays. *IET Generation, Transmission and Distribution*, 11(2):719–729, 2017.

H. Gunduz, S. Sonmez and S. Ayasun. The Impact of Electric Vehicles Aggregator on the Stability Region of Micro-Grid System with Communication Time Delay. *Milan PowerTech*, Milan, Italy, DOI:10.1109/PTC.2019.88109562019: 2019.

Y. Han, K. Zhang, L. Hong and E. A. Alves Coelho. MAS based distributed control and optimization in microgrid and microgrid clusters: A comprehensive overview. *IEEE Transactions on Power Electronics*, 33(8):6488–6508, 2018.

W. Kempton and S. Latendre. Electric vehicles as a new power source for electric utilities. *Transportation Research Part D*, 2(3):157–175, 1997.

K. S. Ko and D. K. Sung. The effect of EV aggregators with time-varying delays on stability of load frequency control systems. *IEEE Transactions on Power Systems*, 33(1):669–680, 2018.

K. S. Ko, W. Lee, P. G. Park and D. K. Sung. Delays-dependent region partitioning approach for stability criterion of linear systems with multiple time-varying delays. *Automatica*, 87:389–394, 2018.

P. Kundur. *Power System Stability and Control*. McGraw-Hill, 1994.

H. Liu, Z. C. Hu, Y. H. Song and J. Lin. Decentralized vehicle-to-grid control for primary frequency regulation considering changing demands. *IEEE Transactions on Power Systems*, 28(3):3480–3489, 2013.

T. Masuta and A. Yokoyama. Supplementary load frequency control by use of a number of both electric vehicles and heat pump water heaters. *IEEE Transactions on Smart Grid*, 3(3):1253–1262, 2012.

Q.Hai. Mean-square delay-distribution-dependent exponential synchronization of discrete-time Markov jump chaotic neural networks with random delay. *Journal of Control Engineering and Applied Informatics*, 23(3): 42–52,2021.

A. Naveed, S. Sonmez and S. Ayasun. Stability Regions in the Parameter Space of PI Controller for LFC System with EVs Aggregator and Incommensurate Time Delays. *1st Global Power, Energy and Communication Conference*, Cappadocia, Turkey; 2019.

A. Naveed, S. Sonmez and S. Ayasun. Impact of Electric Vehicle Aggregator with Communication Time Delay on Stability Regions and Stability Delay Margins in Load Frequency Control System. *Journal of Modern Power Systems and Clean Energy*, DOI:10.35833/MPCE.2019.000244: 1-7.

A. Naveed, S. Sonmez and S. Ayasun. Stability regions in time delayed two area LFC system enhanced by EVs. *Turkish Journal of Electrical Engineering and Computer Science*, In Press:1–14, 2021.

Olle I. Elgerd. *Electrical Energy Systems Theory: An Introduction*. McGraw-Hill, 1971.

H. Gunduz, S.Sonmez and S.Ayasun. Identification of gain and phase margins based robust stability regions for a time-delayed micro-grid system including fractional-order controller in presence of renewable power generation. *Turkish Journal of Electrical Engineering and Computer Sciences*, 30(3):1097–1114,2022.

A. Naveed, S.Sonmez and S.Ayasun. Impact of electric vehicles aggregators with communication delays on stability delay margins of two-area load frequency control system. *Transactions of the Institute of Measurement and Control*, 43(12):2860–2871,2022.

S. B. Pandu, T.Santhanakrishnan, C. K. Sundarabalan, V. Venkatachalam. Stability Analysis and Region in control parameter space of thermal system with constant delays. *Journal of Control Engineering and Applied Informatics*, 23(3): 24–31,2021.

M. A. Oretega-Vazquez, F. Bouffard and Vera Silva. SElectric vehicle aggregator/system operator coordination for charging scheduling and services procurement. *IEEE Transactions on Power Systems*, 28(2):1806–1815, 2013.

S. B. Peterson, J. Apt and J. F. Whitacre. Lithium-ion battery degradation resulting from realistic vehicle and vehicle-to-grid utilization. *Journal of Power Sources*, 195(8):2385–2392, 2011.

K. Ramakrishnan and A. Jawahar. A New Delay-Dependent Stability Criterion for Linear System with Two Time-Invariant Delays.. *Sixth Indian Control Conference*, Indian Institute of Technology, Hyderabad, India, 2019.

A. Sauret and F. Gouaisbaut. On the use of Wirtinger inequalities for time-delay systems. *In: Proceedings of the 10th IFAC Workshop on Time Delay Systems*, North Eastern University, Boston, USA, 2012.

. M. A. Hernández-Pérez, B. del Muro-Cuéllar, M. VelascoVilla, D. F. Novella-Rodríguez, R. A. Garrido-Moctezuma, P. J. García-Ramírez. An improvement on the PI controller for a class of high-order unstable delayed systems: Application to a thermal process. *Journal of Control Engineering and Applied Informatics*, 20(1): 25–35,2018.

S. Sonmez, S. Ayasun and O. Chika. An Exact Method for Computing Delay Margin for Stability of Load Frequency Control Systems With Constant Communication Delays. *IEEE Transactions on Power Systems*, 31(1):370–377, 2016.

E. Sortomme and M. A. El-Sharkwi M A. Optimal charging strategies for unidirectional vehicle-to-grid. *IEEE Transactions on Smart Grid*, 2(1):131–138, 2011.

E. Sortomme and M. A. El-Sharkwi M A. Optimal combined bidding of vehicle-to-grid ancillary services. *IEEE Transactions on Smart Grid*, 3(1):70–79, 2012.

E. Sortomme and M. A. El-Sharkwi M A. Optimal scheduling of vehicle-to-grid energy and ancillary services. *IEEE Transactions on Smart Grid*, 3(1):351–359, 2012.

Stephen Boyd, Laurent El Ghaoui, E. Feron and V. Balakrishnan. *Linear Matrix Inequalities in System and Control Theory*. Volume 15 of Studies in Applied Mathematics, SIAM,

A. Tani, M. B. Camara and B. Dakyo. Energy management in the decentralized generation systems based on renewable energy Ultracapacitors and battery to compensate the wind/load power fluctuations. *IEEE Transactions on Industrial Applications*, 51(2):1817–1827, 2015.

J. Tomic and W. Kempton. Using fleets of electric-drive for grid support. *Journal of Power Sources*, 168(2):459–468, 2007.

S. Vachirasricirikul and I Ngamroo. Robust LFC in a smart grid with wind power penetration by coordinated V2G control and frequency control. *IEEE Transactions*

on Smart Grid, 5(1):371–380, 2014.

Vijay P. Singh, N. Kishor and P. Samuel Coomunication time delay estimation for load frequency control in two-area power system. *Adhoc Networks*, 41:69–85, 2016.

Ana Paula Batista and Fabio Goncalves Jota. Effect of Time Delay Statistical Parameters on the Most Likely Regions of Stability in an NCS. *Journal of Control Engineering and Applied Informatics*, 16(1): 3–11,2014.

M. Yilmaz and P. T. Krien. Review of battery charger topologies charging power levels and infrastructure for plug-in electric and hybrid vehicles. *IEEE Transactions on Power Electronics*, 28(5):2151–2169, 2013.

M. Yilmaz and P. T. Krien. Review of the impact of vehicle-to-grid technologies on distributed systems and utility services. *IEEE Transactions on Power Electronics*, 28(12):5673–5689, 2015.

X. L. Zhu and G. H. Yang. Jensen integral inequality approach to stability analysis of continuous-time systems with time-varying delay. *IET Control Theory and Applications*, 2(6):524–534, 2008.